Multi-scale granular mechanics using MPM x DEM

Sacha Duverger, Jérôme Duriez, Pierre Philippe, Stéphane Bonelli

Multi-scale granular mechanics using MPM x DEM

S. DUVERGER[a], J. DURIEZ[b], P. PHILIPPE[c], S. BONELLI[d]

a. INRAE, Aix Marseille Univ, RECOVER, Aix-en-Provence, France; sacha.duverger@inrae.fr

b. INRAE, Aix Marseille Univ, RECOVER, Aix-en-Provence, France; jerome.duriez@inrae.fr

c. INRAE, Aix Marseille Univ, RECOVER, Aix-en-Provence, France; pierre.phillipe@inrae.fr

d. INRAE, Aix Marseille Univ, RECOVER, Aix-en-Provence, France; stephane.bonelli@inrae.fr

Résumé :

Une méthode numérique multi-échelles est proposée afin de modéliser de manière précise les matériaux granulaires soumis à des chargements importants. En effet, les mécanismes agissant à l'échelle microscopique dans le matériau sont décrits à l'aide de la Méthode des Éléments discrets (DEM), traduisant rigoureusement le comportement du matériau. De plus grandes échelles sont atteintes en couplant la DEM avec la Méthode du Point Matériel (MPM), dévelopée pour des matériaux sujets à de grandes déformations, et dont le comportement dépend de leur histoire. Le couplage MPMxDEM est comparé à une simulation pure DEM contenant 30,000 sphères dans le but d'évaluer la fiabilité et l'efficatité du couplage. Un aperçu du comportement du matériau est donné à différents endroits dans l'échantillon, en tirant profit de la modélisation précise des structures microscopiques par la DEM.

Abstract :

A multi-scale numerical method is proposed to accurately model granular materials under severe loading. Indeed, the material's micro-scale mechanisms are described using the Discrete Element Method (DEM), giving a precise behaviour description. To access larger scale, DEM is coupled with the Material Point Method (MPM) which was developed for history-dependent materials subjected to high deformation. The MPMxDEM coupling is compared to a pure DEM simulation containing 30,000 spheres in order to assess the coupling reliability and efficiancy. Insights are given on how the material behaves at different locations inside the sample, taking advantage of DEM's extensive modelling of the material's microscopic structure.

Mots clefs : Multi-scale, DEM, MPM, granular materials, large deformations

1 Introduction

The intricacies of granular materials require a thorough description of their microscopic features. Constitutive models fail to accurately predict such materials' behaviour when loading paths are non-trivial [1, 2], while a more comprehensive model like DEM effectively handles the material's complexity for any loading condition [3, 4, 5]. Indeed, the involvement of all the material's grains and their contacts in the DEM model makes it quite robust, but it is also what limits its capacities: the computational cost increases drastically with the size of the simulated sample. Different parallelisation processes, such

as OpenMP, allows DEM to be more efficient even though they still require to model all grains in the sample. Besides, they are only efficient to some extent [6], DEM's computational demands are thus still very limiting.

To access larger scales, a possibility is to couple DEM with another method, more permissive in terms of sample sizes' range (typically FEM-like methods, which assume the material's continuity). FEMxDEM coupling has been previously done in 2D [7] or in 3D [8], where FEMxDEM was found to be as accurate and faster than pure DEM simulations. However, this coupling suffers from FEM limitations when the sample is subject to large deformations: its accuracy decreases as the mesh distords. The MPM [9] is a FEM-like method that consider Gauss points (called material points in MPM) to be at arbitrary positions and in different number in their elements. Material points can thus freely move within the material's domain, but the equation of motion is solved on a fixed mesh, making MPM a Lagrangian-Eulerian hybrid method [10] capable of handling large deformations. However, this ambitious task of solving the motion equation using randomly located points in the elements makes the classical MPM somewhat biased. Efforts have been made since to enhance the formulation [11, 12, 13, 14], concentrating on improving the discretisation process either at grid points or material points. Many variations of the classical MPM formulation thus exist and MPM is widely used in various domains, such as geotechnical engineering [15, 16] or computer graphics [17].

Using MPM instead of FEM in the coupling makes it possible to preserve a great accuracy even under severe loading conditions. The MPMxDEM coupling was already studied [18] and found to have the same accuracy as pure DEM, but also to be able of handling large deformations. This paper presents a MPMxDEM quasi-static coupling and aims to characterize its performances in terms of accuracy and computational cost. In order to do so, a triaxial test is performed both in pure DEM and MPMxDEM on the same numerical replica of Camargue's sand [19], using the same computational ressources.

2 MPMxDEM formulation

This section presents how both MPM and DEM are formulated and coupled together.

2.1 MPM formulation

MPM was inspired by the Particle In Cell method (PIC) [10], supposed to take advantage of a Lagrangian-Eulerian formulation to model accurately highly distorted compressible fluids. The original formulation of the MPM [9] aimed at adapting PIC to historic-dependant materials, such as granular materials, by computing the material's behaviour on free, moving points, while keeping the resolution of the motion equation on fixed grid points. Continuous physical quantities are assumed to be defined either from nodes values and shape functions, or material points values and particle characteristic functions. The latter was the subject of an MPM generalization [11], designed to give a better description for the stress tensor.

The equation to be solved can be obtained from the system's conservation of momentum. Considering that any admissible velocity field $\underline{V}^*$ is applied to the system, the virtual work principle is obtained:

$$\int_\Omega \underline{V}^* \rho \frac{d\underline{V}}{dt} d\Omega = \int_\Omega \underline{V}^* \mathrm{div}(\underline{\underline{\sigma}}) d\Omega + \int_\Omega \underline{V}^* \rho \underline{g} d\Omega \tag{1}$$

Where ρ is the density of the material, Ω its domain of definition, $\underline{\underline{\sigma}}$ the stress tensor, $\underline{V}$ is the velocity and $\underline{g}$ is the acceleration due to gravity. Using the divergence theorem and an integration by part, the

different contributions to the motion can be identified:

$$\int_\Omega \underline{V}^* \rho \frac{d\underline{V}}{dt} d\Omega = \int_\Omega \underline{V}^* \rho \underline{g} d\Omega + \int_{\partial\Omega} \underline{V}^* \underline{\underline{\sigma}}\, \underline{n} dS - \int_\Omega \nabla \underline{V}^* : \underline{\underline{\sigma}} d\Omega \tag{2}$$

The right-hand side of the equation corresponds to the sum of the volume forces, surface forces and internal forces, respectively. These integrals are computed on each mesh element using either values on nodes, or values at material points. The velocity, its gradient and the surface forces are described over the whole domain through their value at all nodes $\{v\}$ using shape functions $\{S_v\}$:

$$\underline{V}(\underline{x}) = \sum_v \underline{V}_v S_v(\underline{x}); \qquad \nabla \underline{V}(\underline{x}) = \sum_v \underline{V}_v \nabla S_v(\underline{x}); \qquad \underline{\underline{\sigma}}\, \underline{n}\big|_{\underline{x}} = \sum_v \underline{f}_v^{trac} S_v(\underline{x}) \tag{3}$$

Where any quantity subscripted with $\cdot_v$ is taken at a node v and $\underline{f}^{trac}$ is the external traction imposed on nodes. The stress tensor and density are described over the whole domain through their values at all material points $\{p\}$ using particle characteristic functions $\{\chi_p\}$ being non-zero on domains $\{\Omega_p\}$:

$$\underline{\underline{\sigma}}(\underline{x}) = \sum_p \underline{\underline{\sigma}}_p \chi_p(\underline{x}); \qquad \rho(\underline{x}) = \sum_p \frac{m_p \chi_p(\underline{x})}{\mathcal{V}_p} \tag{4}$$

Where any quantity subscripted with $\cdot_p$ is taken at material point p, m_p is the mass attributed the material point and $\mathcal{V}_p$ is the material point's "volume", defined in the next paragraph. In the classical MPM $\chi_p(\underline{x}) = \delta(\underline{x}_p)$, where δ is a pseudo Dirac function, equal to 1 for $\underline{x} = \underline{x}_p$. This description is not ideal since it is not consistent with the continuous assumption for the stress field's form, but it is still reliable for simple cases with regularly spaced material points.

The term that represents internal efforts in equation 2 requires associating a "volume" to each material points, which is also what allows the determination of a "mass" for a point (i.e. m_p). The classical MPM or contiguous GIMP determine these "volumes" by sharing out equally the volume of each mesh's cell between the material points inside. This assumption is acceptable when material points are regularly spaced in their cells, but it becomes wrong as soon as the material points rearrange into an irregular structure. The material points "volumes", along with the particle characteristic functions and the shape functions, constitute what corresponds to the weighting functions for a numerical integration of the internal efforts term. The volume of each material point will be denoted $\mathcal{V}_p$, not to be confused with the velocity at the material points V_p.

With the adopted discretisation process, the internal and external forces can be computed on each node ($\underline{f}_v^{int}$ and $\underline{f}_v^{ext}$ respectively):

$$\underline{f}_v^{int} = -\sum_p \mathcal{V}_p \underline{\underline{\sigma}}_p \cdot \int_{\Omega_p \cap \Omega} \nabla S_v(\underline{x}) \chi_p(\underline{x}) d\underline{x} \tag{5}$$

$$\underline{f}_v^{ext} = \sum_v \underline{f}_v^{trac} + \sum_p m_p \underline{g} \int_{\Omega_p \cap \Omega} S_v(\underline{x}) \chi_p(\underline{x}) d\underline{x} \tag{6}$$

The total force on nodes will be denoted $\underline{f}_v$. A mass can also be attributed to nodes using the shape

functions and the material points' "mass":

$$m_v = \sum_p m_p S_v(\underline{x}_p) \tag{7}$$

Introducing Cundall's damping through a parameter D, the equation of motion can then be solved by computing the acceleration on nodes:

$$\underline{a}_v = \frac{1}{m_v}\left(\underline{f}_v - D\|\underline{f}_v\|\frac{\underline{V}_v}{\|\underline{V}_v\|}\right) \tag{8}$$

The new material points' velocities and positions can finally be determined:

$$\underline{V}_p(t+\Delta t) = \underline{V}_p(t) + \Delta t \sum_v \underline{a}_v(t+\Delta t) S_v(\underline{x}_p(t)) \tag{9}$$

$$\underline{x}_p(t+\Delta t) = \underline{x}_p(t) + \underline{V}_p(t+\Delta t)\Delta t \tag{10}$$

The present scheme used to update $\underline{V}_p$ and $\underline{x}_p$ is called NFLIP (Natural FLuid Implicit Particle method), accelerations are transported from nodes to material points to increment their velocities, which are then used to update their positions [13, 14].

The material's behaviour expresses only through the update of $\underline{\underline{\sigma}}$ using a deformation increment expressed at the material points and computed from the nodal velocities, $\underline{\underline{\dot{\epsilon}}}_p$. Equation 9 makes it clear that the acceleration is updated before the material's point velocities and positions, the behaviour of the material is thus computed from the deformations at the beginning of the time iteration. This stress update scheme is called Update Stress First (USF). The material's response to $\underline{\underline{\dot{\epsilon}}}_p$ is usually computed using constitutive laws, our study uses instead a DEM periodic simulation of a representative volume element (RVE) on which is applied a quasi-static velocity gradient.

2.2 DEM coupling

Each RVE is a sample of $1,000$ poly-disperse spheres, respecting the size distribution of the Camargue's sand given in [19] where a set of contact parameters that includes rolling resistance had been calibrated. Indeed, while using spheres as particles is quite convenient for contact detection and thus computational efficiency, spheres excessively roll between each other and give the material a non-physical lost of resistance. Considering rolling resistance in the contact model effectively corrects this drawback of the sphere model, as shown in [19]. In the present study, the same contact model is used with the same parameters on the same open source software, YADE [20]. The median diameter of the particle size distribution is denoted d_{50} and is $2 \cdot 10^{-4}\ m$.

A sample is generated by creating a cloud of spheres inside a periodic cell on which a spherical velocity gradient is imposed until the sample is compacted to a pressure p consistent with the one considered at the initial stage of the MPM model. During this process, the inter-particle friction angle can be lowered to artificially decrease the force chains' resistance and thus give control on the sample's initial void ratio. A strain increment $\Delta\underline{\underline{\epsilon}}_p = \underline{\underline{\dot{\epsilon}}}_p \Delta t$ is applied to all RVEs during each MPM iteration. A quasi-static deformation time T_p is then computed for all RVE considering a low ratio between inertial forces and

confining forces, i.e. inertial number $I_n = 2.5 \cdot 10^{-4}$ [21]:

$$T_p = \max\left(\frac{\max(\Delta\underline{\underline{\epsilon}}_p)}{I_n}\sqrt{\frac{\rho d_{50}^2}{p}}, \Delta t^{DEM}\right) \tag{11}$$

Where Δt^{DEM} is the DEM time step, computed from contact properties to insure stability of the explicit DEM scheme. A quasi-static strain rate can then be applied to the periodic cell, respecting the final deformation required by the MPM:

$$\dot{\underline{\underline{\epsilon}}}_p^{DEM} = \frac{\Delta\underline{\underline{\epsilon}}}{T_p} \tag{12}$$

After deforming the periodic cell at the rate $\dot{\underline{\underline{\epsilon}}}_p^{DEM}$ for a duration of T_p, the new stress tensor is then computed using Love-Weber formula [22] on each RVE and $\underline{\underline{\sigma}}$ is finally sent back to the MPM.

This MPMxDEM coupling is implemented using the open source softwares CB-Geo MPM [23] and YADE DEM [20], it supports OpenMP parallelisation on the MPM side by distributing all iterations over particles, nodes, and cells to a user defined number of CPU cores.

3 Simulations and results

A simple element test triaxial test is performed in order to ascertain the MPMxDEM capacity to accurately model granular materials. The only MPM cell is a cube with a length $l = 1\ m$, in which 8 material points (more precisely RVEs) are regularly spaced. In the x and y directions, forces are imposed on all nodes oriented toward the sample in order to maintain the confining pressure $p = 100\ kPa$. In the z direction, the bottom nodes velocities are forced to be nil, while on the top nodes a velocity is imposed downwards. This velocity respect quasi-staticity as it is computed from the previously introduced inertial number I_n:

$$V_v^z = -I_n\sqrt{\frac{p}{\rho}} \tag{13}$$

Note that since a constant velocity is imposed on all nodes in the z direction, vertical acceleration is nil everywhere in the domain and thus material points only move horizontally. Also, even though the initial velocity on the top nodes is not zero, the initial velocity of the material points is. That is in fact a trick to limitate the material points' displacement in order to keep the computation of the internal efforts as correct as possible. The physical meaning of the simulation doesn't suffer from such a trick since the MPM considers the material to be present in the whole MPM cell as long as material points are inside. Their positions are then only relevant to compute their "integration weights" but not to determine the material's behaviour, which requires only a consistent value for $\dot{\underline{\underline{\epsilon}}}_p$.

As a reference, a pure DEM simulation was performed on a sample of $30,000$ spheres, to allow the analysis of the coupling's accuracy as well as its efficiency for this simple 8 material points simulation. The pure DEM triaxial test uses the same conditions as each RVE of the previous MPM calculation: both are periodic simulations and their particle size distribution, contact model and sample's initial density are identical. The initial density was measured inside a sub-volume within the sample to avoid any boundary effects. The deformation rate imposed in pure DEM is the same as the one imposed by the MPM on all RVEs, i.e., the one computed with $I_n = 2.5 \cdot 10^{-4}$. Both simulations were run independently on the same machine having an Intel(R) Xeon(R) Platinum 8270 CPU @ 2.70GHz with 1.5 TiB of RAM available, using OpenMP parallelisation on 8 CPU cores.

	Number of particles	Initial void ratio	Computational time cost
Pure DEM	$30,000$	≈ 0.563	≈ 6 hours 43 minutes
MPMxDEM	$1,000$	≈ 0.558	≈ 55 minutes

Table 1: Simulation's initial conditions and computational time cost for both simulations

Table 1 summarises the initial conditions and computation times for both the pure DEM and MPMxDEM simulations. Figure 1 (a) shows the mean deviatoric stress $\overline{q}$ and mean volumetric strain $\overline{\epsilon}_V$ over all RVEs for the MPMxDEM simulation, or computed using the stress tensor and cell deformation for the pure DEM simulation. For this triaxial test, MPMxDEM is approximately 7.3 times faster than pure DEM. As for the accuracy, figure 1 shows that the deviatoric stress is almost the same for both simulations, specially during the low deformations part. However, beyond the maximum stress state the MPMxDEM $\overline{\epsilon}_V$ progressively deviates downwards from the pure DEM $\overline{\epsilon}_V$, but it seems to reach more clearly the critical state. When looking at these mean values, results are consistent since the MPMxDEM is in close agreement with pure DEM regarding the stress response while the computational cost is significantly lower.

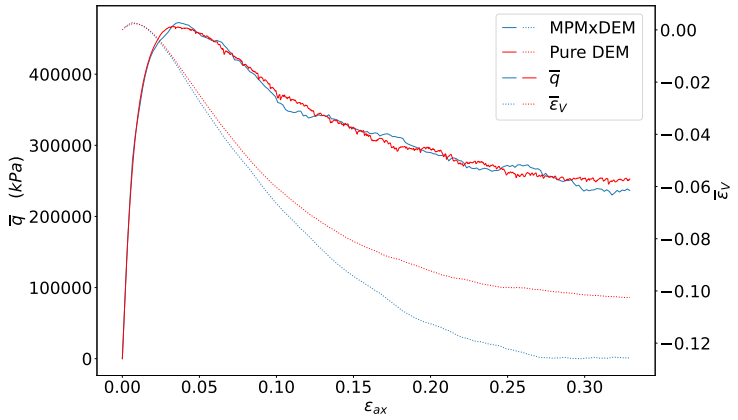

Figure 1: Mean deviator stress $\overline{q}$ and volumetric strain $\overline{\epsilon}_V$ against mean axial strain $\overline{\epsilon}_{ax}$

However, figure 2 (a) shows that during the MPMxDEM simulation (see figure 2 (d) for the RVEs colors and initial position). After the maximum stress state is reached, the control of the lateral stress is lost: half of the RVEs have their lateral stresses decreasing, the other half have them increasing. An interesting point to notice is that none of the RVEs behaves as one of its closest neighbour, and yet there is only two different types of behaviours. This curious arrangement is probably simply the expression of some shape functions' geometrical property. Figure 2 (c) show that the ratio between the axial and lateral stresses is homogeneous for all RVEs during the whole test.

Figure 3 shows the normal and shear stress for two neighbour RVEs (n°1 and n°3). RVE n°3 supports no stress while RVE n°1 is strongly solicatated.

Contrary to the stress tensor, the average coordination number $\overline{Z}_c$ is homogeneous in the MPM cell, as shown on figure 2 (b): all RVEs have about the same $\overline{Z}_c$, exactly for low deformations and more approximately for high deformations.

The incapacity of MPMxDEM to keep the lateral stress constant, as shown in figure 2 (a), is most probably due to the horizontal displacements of the RVEs that increases the "numerical integration's

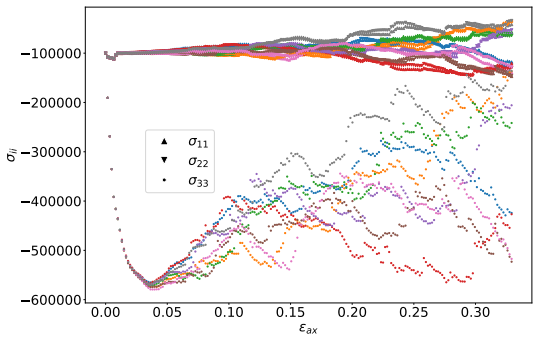

(a) Principal stresses σ_{ii} against axial strain ϵ_{ax}

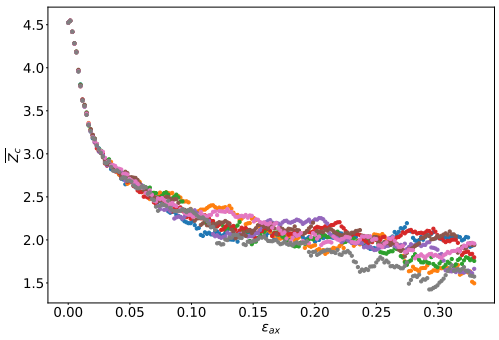

(b) Average number of coordination

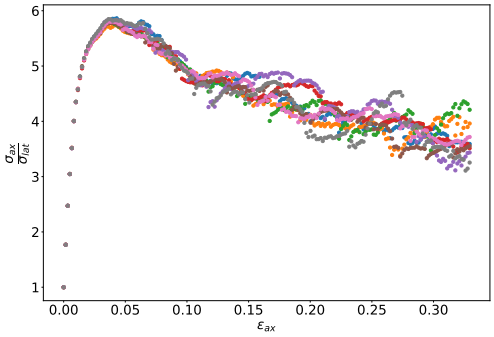

(c) Axial stress σ_{ax} over lateral stress σ_{lat} against axial strain ϵ_{ax}

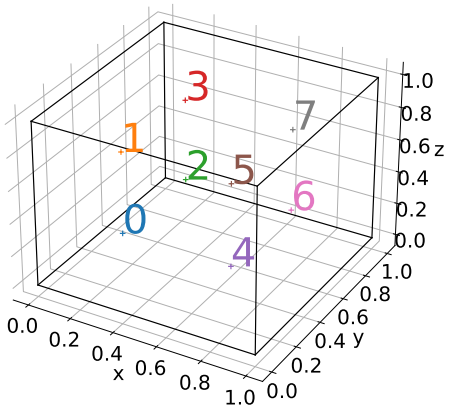

(d) RVE initial positions, colors and numbering

Figure 2: Results for each RVE

weights" error. Indeed, as the particles move, their attributed volume become more and more biased and the computation of the internal efforts becomes false.

4 Conclusion

This study presented a formulation of the MPMxDEM coupling that, even though it suffers from the MPM's imperfect description of the stress tensor, is able to accurately predict the behaviour a granular material subject to high deformations (over 0.3). The obtained deviatoric stress corresponds exactly to the pure DEM response. Other MPM formulations could certainly be considered to improve this coupling, in particular to simulate problems where the material points move significantly.

Data was tracked for all RVEs, giving insights on how the critical stress is sustained by the sample: it appears that less than half the DEM particles are enough to maintain the stress within the sample. The axial and lateral stress ratio as well as the coordination number was shown to be homogeneous between all RVEs. The computational efficiency of the MPMxDEM is quite remarkable considering its accuracy. Indeed, the MPMxDEM simulation presented in this study is approximately 7.3 times faster than a pure DEM reference simulation. A more complex simulation would probably show an even better performance of MPMxDEM with respect to DEM, taking advantage of the scale range MPM makes accessible.

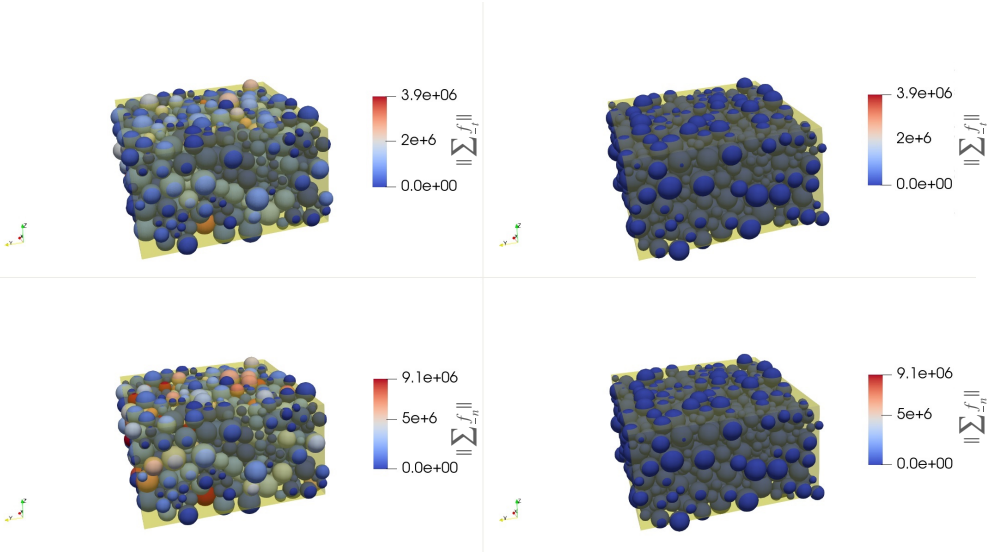

Figure 3: Two RVEs final stress states. The left column is a RVE whose lateral stress decreases (RVE n°1), the right column is a RVE whose lateral stress increases (RVE n°3). $\|\sum \underline{f}_n\|$ (respectively $\|\sum \underline{f}_t\|$) is defined for each particle as the sum on all its interaction forces of the normal (respectively tangential) component divided by the projection of the smallest interacting particle.

References

[1] A. S. Saada and G. Bianchini, "Constitutive equations for granular non-cohesive soils," in *International Workshop on Constitutive Equations for Granular Non-cohesive Soils (1987: Cleveland, Ohio)*, AA Balkema, 1989.

[2] L. Sibille, N. Benahmed, and F. Darve, "Constitutive response predictions of both dense and loose soils with a discrete element model," *Computers and Geotechnics*, vol. 135, p. 104161, 2021.

[3] T. Mohamed, J. Duriez, G. Veylon, and L. Peyras, "Dem models using direct and indirect shape descriptions for toyoura sand along monotonous loading paths," *Computers and Geotechnics*, vol. 142, p. 104551, 2022.

[4] Y. Zhang, J. Shao, Z. Liu, C. Shi, and G. De Saxcé, "Effects of confining pressure and loading path on deformation and strength of cohesive granular materials: a three-dimensional dem analysis," *Acta Geotechnica*, vol. 14, no. 2, pp. 443–460, 2019.

[5] M. Jiang, F. Zhang, and Y. Sun, "An evaluation on the degradation evolutions in three constitutive models for bonded geomaterials by dem analyses," *Computers and Geotechnics*, vol. 57, pp. 1–16, 2014.

[6] J. Duriez and S. Bonelli, "Precision and computational costs of level set-discrete element method (ls-dem) with respect to dem," *Computers and Geotechnics*, vol. 134, p. 104033, 2021.

[7] T. K. Nguyen, G. Combe, D. Caillerie, and J. Desrues, "Fem× dem modelling of cohesive granular materials: numerical homogenisation and multi-scale simulations," *Acta Geophysica*, vol. 62, no. 5, pp. 1109–1126, 2014.

[8] Y. Liu, W. Sun, Z. Yuan, and J. Fish, "A nonlocal multiscale discrete-continuum model for predicting mechanical behavior of granular materials," *International Journal for Numerical Methods in Engineering*, vol. 106, no. 2, pp. 129–160, 2016.

[9] D. Sulsky, Z. Chen, and H. L. Schreyer, "A particle method for history-dependent materials," *Computer methods in applied mechanics and engineering*, vol. 118, no. 1-2, pp. 179–196, 1994.

[10] F. H. Harlow, "The particle-in-cell method for numerical solution of problems in fluid dynamics," tech. rep., Los Alamos Scientific Lab., N. Mex., 1962.

[11] S. G. Bardenhagen and E. M. Kober, "The generalized interpolation material point method," *Computer Modeling in Engineering and Sciences*, vol. 5, no. 6, pp. 477–496, 2004.

[12] A. de Vaucorbeil, V. P. Nguyen, S. Sinaie, and J. Y. Wu, "Material point method after 25 years: Theory, implementation, and applications," *Advances in applied mechanics*, vol. 53, pp. 185–398, 2020.

[13] A. Stomakhin, C. Schroeder, L. Chai, J. Teran, and A. Selle, "A material point method for snow simulation," *ACM Transactions on Graphics (TOG)*, vol. 32, no. 4, pp. 1–10, 2013.

[14] Y. Fei, Q. Guo, R. Wu, L. Huang, and M. Gao, "Revisiting integration in the material point method: a scheme for easier separation and less dissipation," *ACM Transactions on Graphics (TOG)*, vol. 40, no. 4, pp. 1–16, 2021.

[15] K. Soga, E. Alonso, A. Yerro, K. Kumar, and S. Bandara, "Trends in large-deformation analysis of landslide mass movements with particular emphasis on the material point method," *Géotechnique*, vol. 66, no. 3, pp. 248–273, 2016.

[16] C. Coetzee, P. Vermeer, and A. Basson, "The modelling of anchors using the material point method," *International journal for numerical and analytical methods in geomechanics*, vol. 29, no. 9, pp. 879–895, 2005.

[17] C. Jiang, C. Schroeder, J. Teran, A. Stomakhin, and A. Selle, "The material point method for simulating continuum materials," in *ACM SIGGRAPH 2016 Courses*, pp. 1–52, 2016.

[18] W. Liang and J. Zhao, "Multiscale modeling of large deformation in geomechanics," *International Journal for Numerical and Analytical Methods in Geomechanics*, vol. 43, no. 5, pp. 1080–1114, 2019.

[19] R. Aboul Hosn, L. Sibille, N. Benahmed, and B. Chareyre, "Discrete numerical modeling of loose soil with spherical particles and interparticle rolling friction," *Granular matter*, vol. 19, no. 1, pp. 1–12, 2017.

[20] V. Smilauer *et al.*, *Yade Documentation 3rd ed.* The Yade Project, 2021. http://yade-dem.org/doc/.

[21] F. Da Cruz, S. Emam, M. Prochnow, J.-N. Roux, and F. Chevoir, "Rheophysics of dense granular materials: Discrete simulation of plane shear flows," *Physical Review E*, vol. 72, no. 2, p. 021309, 2005.

[22] F. Nicot, N. Hadda, M. Guessasma, J. Fortin, and O. Millet, "On the definition of the stress tensor in granular media," *International Journal of Solids and Structures*, vol. 50, no. 14, pp. 2508 – 2517, 2013.

[23] K. Kumar, J. Salmond, S. Kularathna, C. Wilkes, E. Tjung, G. Biscontin, and K. Soga, "Scalable and modular material point method for large-scale simulations," *arXiv preprint arXiv:1909.13380*, 2019.